Contents lists available at ScienceDirect

Applied Surface Science

journal homepage: www.elsevier.com/locate/apsusc

Full Length Article

Theory-guided design of Pd/C nanocomposite for H_2 sensing at room-temperature

Yang Gao [a], Qiao Lu [a], Peijian Yan [a], Pengfei Tian [a,*], Minghui Zhu [b], Biao Xiao [c], Fuzhen Xuan [a,*]

[a] Key Laboratory of Pressure Systems and Safety, Ministry of Education, School of Mechanical and Power Engineering, East China University of Science and Technology, Shanghai 200237, China
[b] State Key Laboratory of Chemical Engineering, School of Chemical Engineering, East China University of Science and Technology, Shanghai 200237, China
[c] Shanghai Institute of Special Equipment Inspection and Technical Research, Shanghai 200062, China

A B S T R A C T

Palladium (Pd) has attracted widespread attention in the application of hydrogen gas (H_2) sensors. Understanding the effect of surface structure on H_2 activation is central to controlling H_2 sensing performance. Here we use density functional theory (DFT) to investigate the adsorption and activation of H_2 on Pd surfaces including (100), (110) and (111). The most stable adsorption configuration of H_2 with the lowest dissociative adsorption energy of -0.960 eV and the charge transfer of -0.126 e from Pd to H was found on the hexagonal close-packed (hcp) site of Pd(111), suggesting that Pd(111) is most favorable for hydrogen sensing. Consistent with theoretical predication, the designed Pd nano-octahedrons enclosed by Pd(111) facets, which was synthesized by solution reduction method and characterized by multi-techniques including field emission scanning electron microscope (FESEM) and transmission electron microscope (TEM), manifested a high sensitivity of 0.1%, a short response/recover time of 35.5/40.2 s to 4000 ppm H_2 and great stability (15 cycles towards 4000 ppm H_2). Accordingly, we propose that the facile dissociative adsorption of H_2 on Pd(111) contributes to the readily formation of PdH_x and the rapid resistance change, thus leading to the superior performance for H_2 sensing.

1. Introduction

With the trend of reducing the utilization of fossil energy and achieving carbon neutrality, the market demand of hydrogen fuel cell vehicles (HFCV) is increasing, since hydrogen (H_2) is considered to be the most effective and environmental-friendly renewable energy due to its low ignition energy (0.017 mJ), high combustion heat (142 kJ/g), no carbon emissions and abundant raw materials [1–3]. However, H_2 is intrinsically flammable and explosive within a wide explosion range (4–75%), and leaks easily because of the vibration, collision and fatigue of HFCV during service [4–7]. Therefore, the development of high-sensitivity and fast-response room-temperature hydrogen gas sensors is critical and essential for the accurate and rapid detection of hydrogen leakage during the usage of H_2 in hydrogen vehicles.

Various gas-sensing materials have been explored for the detection of hydrogen, including noble metals, alloys, metal oxide semiconductors and noble metal decorated composites [8–12]. Among them, Pd is considered to be the most potential room-temperature sensing material for H_2 sensors due to its superior capacity for the adsorption and activation of H_2 on its surfaces, and consequently Pd-based hydrogen gas sensors have been widely investigated and applied in many fields such as hydrogen production, hydrogen storage and hydrogen vehicles [13–15]. Pd nanowires (NWs) [16,17] and nanoparticles (NPs) loading on various supports including WO_3 [18], ZnO [19], carbon nanotube [20] and reduced graphene oxide [21] have proved to be effective for H_2 sensing. Especially, carbon black is extensively used as a conductive support due to its high surface area, great electrical conductivity and low cost, which can provide abundant loading sites for Pd NPs and has great potential for gas-sensing applications [22]. In addition to monometallic Pd, Pd-based alloys such as PdAg [23] and PdAuCu [24] have also shown superior sensing performance. Although Pd-based nanomaterials have been extensively studied, few Pd-based H_2 sensors reported have achieved the performance metrics announced by the U.S. Department of Energy (DOE) [25]. It is still challenging to obtain H_2 sensors with high selectivity, short response time, great stability and wide concentration range for H_2 detecting at room temperature [26]. Poor understanding in the structure-performance relationship of Pd active sites and the mechanism for H_2 sensing restrains the rational design of high-performance H_2

---

sensors, raising the need for theoretical studies at molecular level.

A thorough understanding of the interaction mechanism between Pd and H_2 is of vital importance to the development of high-performance Pd-based hydrogen gas sensors. First-principles calculations have been found to be effective approaches to probe sensing mechanism of sensor materials [27]. To date, theoretical studies of Pd-based H_2 sensors focused on the supported Pd nanomaterials such as Pd-doped MoS_2 [28], Pd decorated graphene [29] and Pd doped ZnO [30], which revealed the critical role of Pd in the nanocomposites for H_2 sensing. According to previous studies, the sensing process of resistive Pd-based H_2 sensors could be proposed as follows: H_2 molecules are dissociative adsorbed on the Pd surfaces, then diffuse into to the palladium crystal to form PdH_x, which leads to a change in resistance of sensors [31–33]. Hence, the understanding of the role of the surface structure in H_2 sensing is crucial for the rational design of H_2 sensors. Although plenty theoretical studies on Pd-based sensors have been reported, there is still a lack of profound research and understanding of the structure-activity relationship between Pd surface structure and hydrogen sensing performance, hindering the development of high-performance hydrogen gas sensors.

In this study, we aim to investigate the structure-performance correlation of typical Pd surfaces and thus realize the theory-guided rational design of Pd-based H_2 sensors. The adsorption and dissociative activation of H_2 on Pd surfaces including (1 0 0), (1 1 0) and (1 1 1) were theoretically investigated using density functional theory (DFT) calculations. Pd(1 1 1) was proved to have the most potential for H_2 sensing. Guided by theoretical results, carbon black supported Pd nano-octahedrons enclosed by Pd(1 1 1) facets was successfully synthesized by solution reduction method and dripped on the Cu interdigital electrode to fabricate H_2 sensors. The gas-sensing performance was measured at room temperature towards various H_2 concentrations. The mechanism of the hydrogen gas sensor was discussed according to the theoretical and experimental results.

2. Methods

2.1. Computational details

All theoretical calculations were performed by the Vienna ab initio simulation package (VASP) [34], which is based on DFT using projector augmented wave (PAW) [35] pseudopotentials. The exchange correlation functional was described by the generalized gradient approximation (GGA) method with the Perdew − Burke − Ernzerhof (PBE) version [36]. The plane-wave energy cutoff and the energy convergence criterion were set to 500 eV and 1×10^{-5}, respectively. A 2×2 unit cell with a slab of five layers was employed for the three Pd surfaces including (1 0 0), (1 1 0) and (1 1 1). The thickness of the vacuum layer perpendicular to these surfaces is larger than 20 Å to avoid the interaction between layers. A $5 \times 5 \times 1$ Monkhorst − Pack k-point grid in Brillouin zone was used for the relaxation calculations, while a $15 \times 15 \times 1$ Monkhorst − Pack k-point grid was used for the self-consistent procedures [37]. To evaluate the interaction between H_2 and different Pd surfaces, the adsorption energy (E_{ads}) is defined as:

$$E_{ads} = E_{Pdsurface+H_2} - E_{Pdsurface} - E_{H_2} \tag{1}$$

where $E_{Pdsurface+H_2}$ is the total energy of the Pd surface with an adsorbed H_2 molecule, and $E_{Pdsurface}$ and E_{H_2} are the total energies of the Pd surface and a single H_2 molecule, respectively.

Charge density difference (CDD) after H_2 adsorption is defined as:

$$\Delta\rho = \rho_{Pdsurface+H_2} - \rho_{Pdsurface} - \rho_{H_2} \tag{2}$$

where $\rho_{Pdsurface+H_2}$ is the total charge density of the Pd surface with an adsorbed H_2 molecule, and $\rho_{Pdsurface}$ and ρ_{H_2} are the total charge densities of the Pd surface and a single H_2 molecule, respectively.

To further analyze the interaction, we calculated the density of states

(DOS) and the Bader charge [38] which is used to evaluate the charge transfer during the adsorption process.

2.2. Materials

Palladium chloride ($PdCl_2$), 1-octadecene (greater than90%), oleylamine (80–90%), n-butyllithium solution (2.2 M in cyclohexane), cyclohexane and carbon black were obtained from Macklin. Ferric chloride ($FeCl_3$) was purchased from Sinopharm Chemical Reagent Shanghai Co., Ltd. Flexible copper clad PI films with thickness of 50 μm were purchased from Kunshan Spring Rhyme Optical Materials Co. Ltd. All the chemicals were used without further purification.

2.3. Synthesis of Pd/C nanocomposite

The Pd nano-octahedrons were prepared according to the following procedure [39,40]. Butyllithium and oleylamine were used as reducing and stabilizing agents, respectively. The precursor solution was acquired by adding 0.1 mmol Pd chloride to the mixture of 15 mL 1-octadecene, 1 mL butyllithium and 2 mL oleylamine. The mixed solution was stirred at 80 °C for 20 min. Then, the mixture was further aged at 150 °C for 2 h. The obtained mixture was cooled down to room temperature and centrifuged with methanol and acetone several times to collect monometallic Pd nano-octahedrons.

The obtained black monometallic Pd nano-octahedrons were further re-dispersed in cyclohexane to get the colloid of Pd nano-octahedrons, and a calculated amount of commercial carbon black powder was added into the above colloid to achieve a metallic Pd loading of 1.0 wt%. The obtained mixture was then heated to 60 °C and purged with N_2 to remove cyclohexane to obtain the black Pd/C products, which was further washed by acetone and methanol several times to completely remove the residues of surfactant impurities. The obtained products were finally washed with acetone and air-dried for further gas-sensing applications.

2.4. Fabrication of H_2 sensor

The Cu interdigital electrode on a flexible PI film were fabricated by the inkjet printing method, where the ink serving as a mask was printed on Cu-clad PI film to gain an interdigital pattern and dried for 10 min, then the unmasked parts of Cu-clad PI films were etched by $FeCl_3$ solution in deionized water (1 mM). To obtain homogeneous dispersion, 1 g as-synthesized Pd/C nanocomposite was dispersing in 1 mL alcohol with ultrasonic treatment for 1 h. The dispersion was then dripped between the interdigital electrodes, and dried in the air to fabricate hydrogen gas sensors.

2.5. Material characterization

The microstructure and morphology of Pd/C nanocomposite were observed by field emission scanning electron microscope (FESEM, GeminiSEM500) and transmission electron microscope (TEM, JEM 2100F). The elemental compositions and elemental mappings were obtained on an energy dispersive spectrometer (EDS, Falion 60S). To characterize the chemical compositions and chemical state of Pd/C nanocomposite, X-ray photoelectron spectroscopy (XPS) was carried out on a Thermo Fisher Scientific K-Alpha.

2.6. Gas-sensing performance test

The H_2 gas-sensing measurement of the Pd/C nanocomposite based gas sensors was carried out at room temperature towards 2000–12000 ppm H_2. The components of the measurement system are PTFE chamber, gas distribution instrument, gas transmission line and electrochemical workstation. To obtain gas-sensing performance accurately, the different volume of 2% H_2 and pure N_2 are mixed in gas distribution

instrument to obtain the required H_2 concentration and transmitted to the chamber. Simultaneously, the real-time gas response is detected by electrochemical workstation.

The gas sensor sensitivity (S) is defined as:

$$S(\%) = (R_g - R_a)/R_g \times 100 \tag{3}$$

where R_g and R_a are the resistances of the gas sensor in target gas and dry air, respectively. The response time (τ_{res}) is defined as the time from initial resistance to 90% of the saturation resistance, while the recovery time (τ_{rec}) is defined as the time from saturation resistance to 10% of the initial resistance for the gas sensors. The stability of the gas sensors was characterized by several response-recovery cycles at the same gas concentration.

3. Results and discussion

3.1. Chemical dissociative adsorption of H_2 on the Pd surfaces

To understand the effect of surface structure on the performance of H_2 sensing, theoretical calculations were carried out to investigate the adsorption and activation behaviors of H_2 on Pd surfaces and their potentialities for the application in H_2 sensors. Three typical low Miller index Pd surfaces including (1 0 0), (1 1 0) and (1 1 1) were studied thoroughly. Based on the vibrational analysis [41], the frequency of Pd (1 0 0), Pd(1 1 0) and Pd(1 1 1) ranges from 17.26 to 213.91, 35.31 to 219.69 and 18.76 to 221.40 cm^{-1}, respectively, demonstrating great chemical stability of three pristine Pd surfaces. All possible adsorption sites of H_2 on Pd surfaces were considered, as shown in Fig. 1a-c marked in yellow, including the top (T) site over the fist layer of Pd atoms, the bridge (B) site and the hollow (H) site. Moreover, due to the different
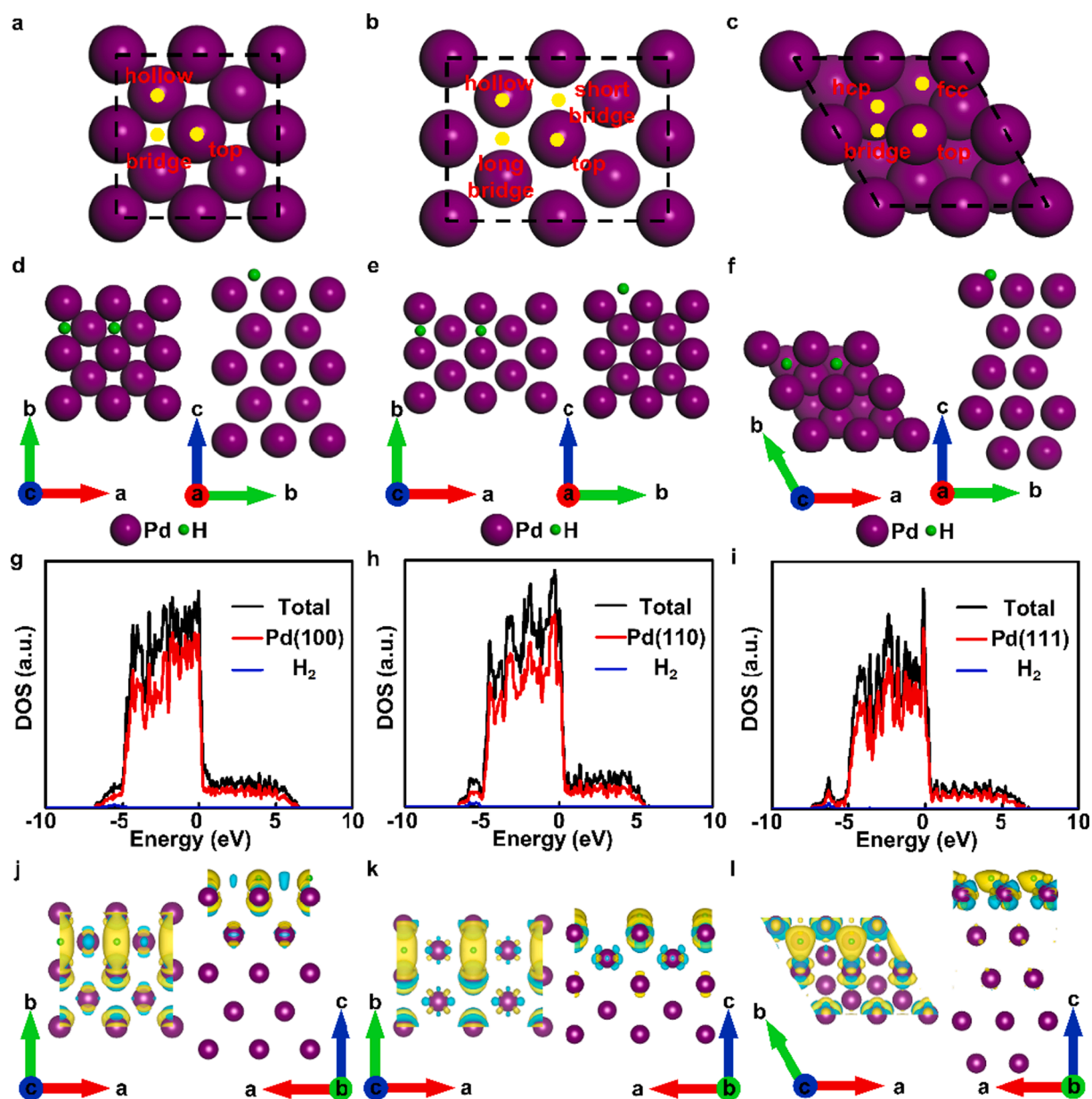

Fig. 1. Schematic diagram of typical adsorption sites for a single H_2 molecule on the (a) Pd(1 0 0), (b) Pd(1 1 0) and (c) Pd(1 1 1) from the top view. The most stable adsorption configuration of H_2 on the (a) Pd(1 0 0), (b) Pd(1 1 0) and (c) Pd(1 1 1) from the top view and side view. PDOS spectra of the adsorbed H_2 molecule on the (g) Pd(1 0 0), (h) Pd(1 1 0) and (i) Pd(1 1 1). Fermi level corresponds to zero. The Charge density difference (CDD) of adsorbed H_2 molecule on the (j) Pd(1 0 0), (k) Pd (1 1 0) and (l) Pd(1 1 1) from the top view and side view. The yellow region represents electron gain, while the blue region represents electron loss.

structure of three Pd surfaces, the short bridge (SB) site and the long bridge (LB) site of Pd(1 1 0) as well as the hexagonal close-packed (hcp) site and the face-centered cubic (fcc) site of Pd(1 1 1) were involved. The corresponding adsorption energies are displayed in Table.1.

The most stable configurations with the lowest E_{ads} value are presented in Fig. 1**d-f** from the top view and the side view, corresponding to the H site of Pd(1 0 0), H site of Pd(1 1 0) and hcp site of Pd(1 1 1). The distance between the two H atoms of H_2 on Pd(1 0 0), Pd(1 1 0) and Pd (1 1 1) increases to 2.702, 3.730 and 2.744 Å, respectively, from the initial distance of 0.750 Å in gas phase, and the shortest distance between H and Pd surfaces is 1.024, 0.987 and 0.873 Å, respectively (Table.1), which indicates the fracture of H-H bond and the formation of Pd-H bonds. In case of the typical chemisorption process, the H_2 molecule dissociated into two H atoms, and are bonded to two adjacent Pd atoms, which is the critical step for the formation of PdH_x. Among the three Pd surfaces, the lowest E_{ads} of −0.960 eV was found in hcp site of Pd(1 1 1) attributed to the lowest d_{H-S} of 0.873 Å and the largest atomic density.

To clarify electronic interaction between H_2 and Pd surfaces, we calculated the DOS of the most stable configurations. As depicted in Fig. 1**g-i**, the total DOS near the Fermi level, which is set to 0 eV, was dominated by Pd. The overlapping part of partial density of states (PDOS) near 5 eV of H atoms and Pd surfaces indicates that the hydrogen atom and the Pd atom are hybridized, which would affect the conductivity of metallic Pd. To qualitatively and quantitatively investigate the charge transfer during the process of H_2 adsorption on Pd surfaces, the CDD and Bader charge transfer (C_T) were calculated. As shown in Fig. 1**j-l**, the yellow region representing electron gain surrounds the H atoms, revealing that the charge is transferred from the Pd surface to the H atoms, corresponding to a negative C_T value for H (Table.1). The charge transfer between Pd and H depends on whether H_2 molecules dissociate and the distance between H and Pd surfaces, which would determine the change of the conductivity of metallic Pd. The Bader charge transfer from Pd to H for the most stable adsorption of H_2 on Pd(1 0 0), Pd(1 1 0) and Pd(1 1 1) is −0.132, −0.153 and −0.126 e respectively (Table.1), which would decrease the conductivity of metallic Pd.

Accordingly, among the three low-Miller-index surfaces, Pd(1 1 1) with the largest capacity for H_2 adsorption is most favorable for H_2 sensing. The charge transfer from Pd to H during the dissociative adsorption and activation of H_2 plays a critical role in decreasing the conductivity of metallic Pd, thus leading to the increase in resistance of the Pd-based resistive gas sensor when exposed to hydrogen.

3.2. Structural characterization of Pd/C nanocomposite

Guided by theoretical results, Pd/C nanocomposite was synthesized by solution reduction method to obtain the Pd particles with (1 1 1) facets, and multi-techniques were utilized to characterize the structure. The FESEM images of as-prepared Pd/C nanocomposite using SE signal

Table 1

The distance between the two H atoms (d_{H-H}), the shortest distance between H atom to Pd surface (d_{H-S}), the adsorption energy (E_{ads}) and the Bader charge transfer (C_T) of H_2 adsorbed on different sites of three Pd surfaces. A negative C_T value signifies electrons transfer from the Pd surface to H_2 molecule.

Surfaces	Sites	d_{H-H} (Å)	h_{H-S} (Å)	E_{ads} (eV)	C_T (e)
Pd (1 0 0)	T	0.869	1.667	−0.299	0.049
	B	0.967	1.212	−0.314	0.032
	H	2.702	1.024	−0.806	−0.132
Pd (1 1 0)	T	0.848	1.700	−0.328	0.033
	LB	0.850	1.516	−0.325	0.031
	SB	0.913	1.320	−0.350	0.009
	H	3.730	0.987	−0.726	−0.153
Pd (1 1 1)	T	0.856	1.693	−0.185	0.045
	B	2.742	0.873	−0.960	−0.125
	hcp	2.744	0.873	−0.960	−0.126
	fcc	2.744	0.822	−0.871	−0.109

and BSE signal are shown in Fig. 2**a-b**. Distinguished according to the lightness of SEM image using BSE signal, there are plentiful irregular spheroids with ca. 50 nm in size and several little bright spots circled in white, which represent the carbon black particles and Pd nanoparticles, respectively. The primary elements of the Pd/C nanocomposite are C, O and Pd (0.73%, Wt), according to the EDS spectrum shown in Fig. 2**c**.

The microstructure of Pd/C nanocomposite was further investigated by TEM shown in Fig. 2**d–e**. The high-resolution TEM image (Fig. 2**d**) and the EDS mapping (Fig. 2**f**) clearly illustrate that the nanosized Pd nanoparticles are evenly dispersed on the carbon black surface. The HRTEM image shows the existence of Pd octahedrons with an average size of ca. 10 nm. The lower-left inset of Fig. 2**e** present that the interplanar distance of a typical Pd octahedron with a great crystalline structure is 0.22 nm, corresponding to the (1 1 1) plane of face-centered-cubic (fcc) Pd crystal, proving that Pd nanoparticles enclosed by Pd (1 1 1) facets was successfully achieved.

In addition, the XPS spectra was used to confirm the chemical composition and electronic states of Pd/C nanocomposite. The XPS spectra in Fig. 2**g** reveals that Pd/C nanocomposite contains O, N, Pd and C elements. As can be seen from the XPS spectra of Pd 3d in Fig. 2**h**, Pd 3d was fitted into two peaks with the binding energies at 335.4 and 340.8 eV, corresponding to the two chemically different spin-orbit pairs (Pd $3d_{5/2}$ and $3d_{3/2}$) [40,42]. Both peaks are characteristic peaks for electron emission from metallic palladium, which reveals the reduction of Pd^{2+} to Pd^0. The C 1 s XPS spectra can be divided into 5 peaks located at 284.8, 285.4, 286.6, 288.2 and 290.1 eV, corresponding to the sp^2 C = C, sp^3 C − C, C − O, C = O species and $\pi − \pi^*$ translation loss [43,44].

3.3. H_2 gas-sensing performance and mechanism

A typical as-fabricated H_2 sensor (Fig. 3**c**) is mainly composed of PI substrate, Pd/C nanocomposite and Cu interdigital electrode. Cu interdigital electrode patched on PI substrate with interdigital spacing of ca. 300 μm and width of ca. 200 μm is shown in Fig. 3**b**. Fig. 4**a** shows the real-time gas response towards 2000–12000 ppm H_2 in N_2 at room temperature. Consistent with the theoretical predication, the designed Pd nano-octahedrons enclosed by Pd(1 1 1) facets, manifested superior performance for H_2 sensing. The resistance of the gas sensor based on Pd/C nanocomposite increases when exposed to hydrogen and is positively correlated with hydrogen concentration. The basically linear relationship between sensitivity and hydrogen concentration was fitted in Fig. 4**b**, in which the sensitivity of the H_2 sensor increases from 0.05% to 0.2% with the hydrogen concentration increasing from 2000 to 12000 ppm.

Fig. 4**c** illustrates a typical gas sensing process towards 4000 ppm H_2, in which the resistance of the Pd/C nanocomposite sensor increases when exposed to H_2 and decreases when departed from H_2. The average response time of 35.5 s is shorter than the average recovery time of 40.2 s, which indicates the hydrogen desorption process is more difficult than its adsorption process. As the hydrogen concentration increases from 2000 to 12000 ppm, both the response time and recover time increase, but gradually tend to be stable (Fig. 4**f**), which demonstrates the H_2 adsorption sites on Pd/C nanocomposite are limited. To study the stability of the hydrogen gas sensors, a cycle test towards 4000 ppm H_2 was carried out (Fig. 4**d**). The sensitivity of each cycle is stable at 0.10% towards 4000 ppm H_2 (Fig. 4**e**), which reveals the H_2 sensor based on Pd/C nanocomposite has extraordinary stability.

Based on the above discussion, we propose that the charge transfer from Pd to H during the dissociative adsorption process of H_2 (Fig. 3**a**), which could lead to the resistance change of H_2 sensor, plays a critical role in H_2 sensing. According to the theoretical results, when the Pd surfaces are exposed to H_2, the H_2 molecule cleaves to two H atoms and bind to Pd atoms, and the PdH_x is formed eventually with the diffusion of H atoms in Pd lattice. The electrons are transferred from Pd atoms to H atoms during adsorption process, and consequently the resistance of metallic Pd increases. Thus, the readily dissociative adsorption of H_2 on
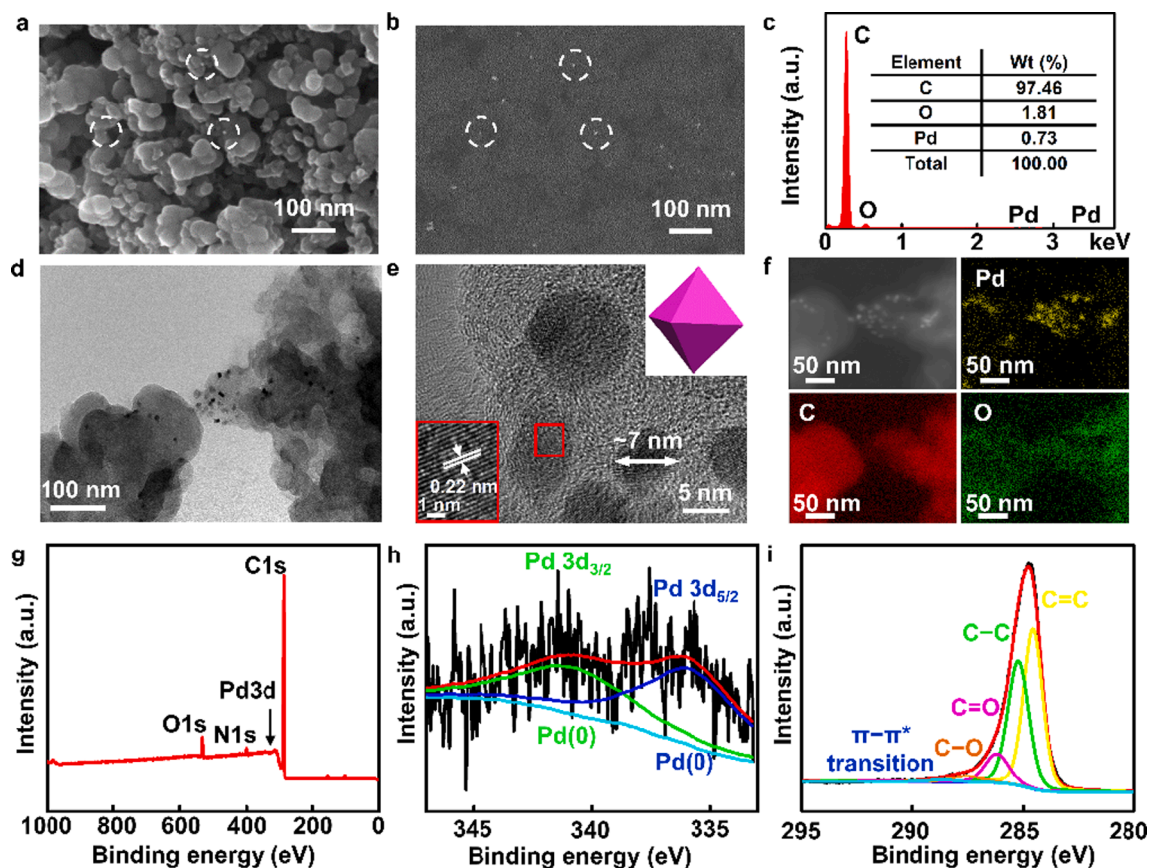
Fig. 2. Microstructure of Pd/C nanocomposite. FESEM image of Pd/C nano-composite using (a) SE signal and (b) BSE signal. (c) EDS spectrum of Pd/C nano-composite. (d) TEM and (e) HRTEM images of Pd/C nanocomposite and (f) the corresponding elemental distribution. (g) XPS spectra of Pd/C nanocomposite. High-resolution XPS spectra of (h) Pd 3d and (i) C 1 s.
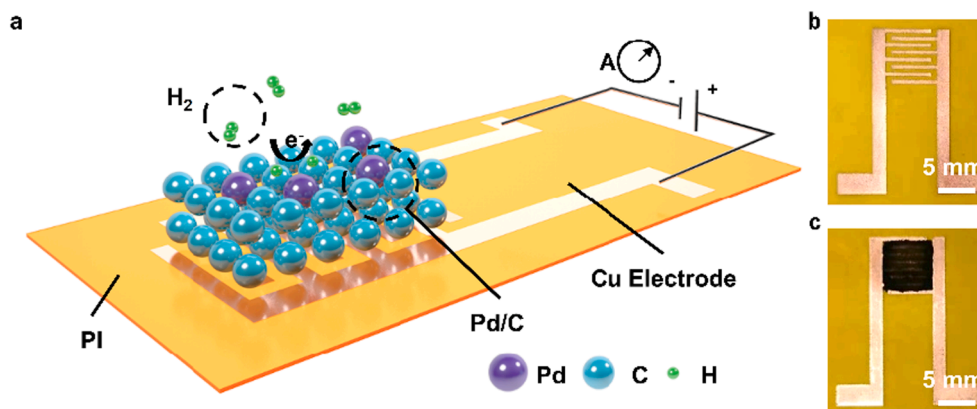

Fig. 3. (a) Schematic diagram of the mechanism of H_2 Sensor. (b) Photograph of as-prepared Cu interdigital electrode on PI film. (c) Photograph of as-fabricated flexible hydrogen gas sensor.

Pd(1 1 1) makes it a superior surface for H_2 sensing. Moreover, the electron transfer between palladium hydride and carbon black also plays an important role in H_2 sensing, as depicted in Fig. 4g, in which the work function of Pd, PdH_x and C were calculated using DFT method [45]. With exposing the sensing material to H_2, due to the facile formation of PdH_x, of which the work function ($W_{PdHx} = 4.3$ eV) [46,47] is much lower than that of carbon black ($W_{carbon\ black} = 5.1$ eV), the electrons are transferred from Pd to carbon black [48,49], leading to the reduction in the concentration of free electrons in metallic Pd and the increase in the resistance of the Pd/C sensors, consistent with our test results. On the other hand, with the release of H_2, the H atoms escape from Pd lattice

and bonds with each other to reform H_2 molecules. Meanwhile, the electrons are transferred back to Pd ($W_{Pd} = 5.3$ eV) [50,51] from carbon black, resulting in the recovery of the resistance of the Pd/C based H_2 sensor.

4. Conclusions

In this work, we present the theory-guided design of Pd/C nano-composite for H_2 sensing at room-temperature. DFT calculations indicate that Pd(1 1 1) surface possess the largest capacity for the dissociative adsorption of H_2 with the lowest adsorption energy (E_{ads}) of
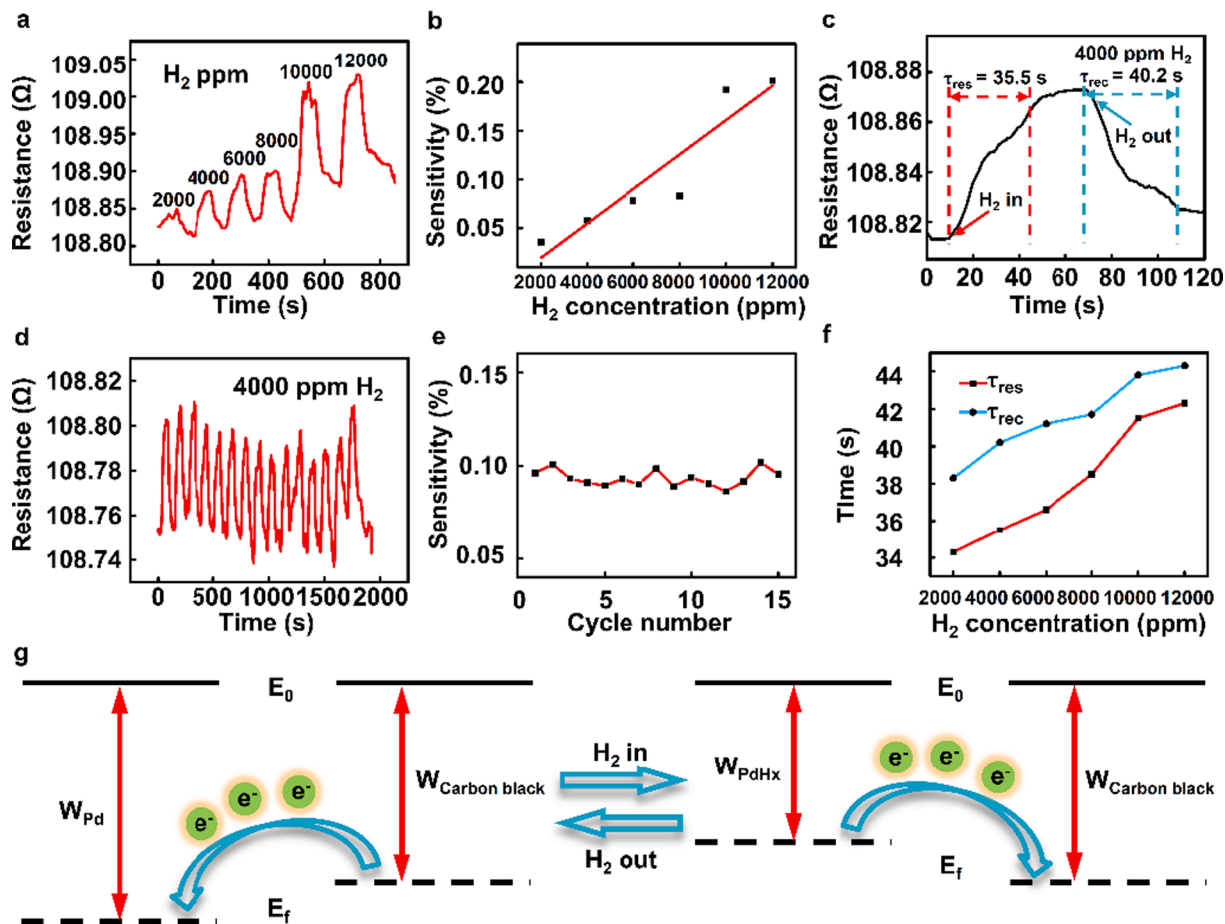
Fig. 4. (a) The gas response curves towards 2000–12000 ppm H_2 in N_2 at room temperature. (b) The sensitivity of the H_2 sensor exposing to different concentrations from 2000 to 12000 ppm. (c) The response/recovery curve towards 4000 ppm H_2. (d) The response/recovery cycle curves towards 4000 ppm H_2. (e) The sensitivity of the H_2 sensor exposing to 4000 ppm H_2. (f) The response/recovery times of the H_2 sensor towards 2000–12000 ppm H_2. (g) The Energy band diagrams of Pd, carbon black and PdH_x before and after H_2 exposure with electron transfer.

−0.960 eV and the charge transfer (C_T) of −0.126 e attributed to the largest atomic density. Suggestively, the Pd(1 1 1) was the most suitable surface for the H_2 gas sensing. The H_2 sensor based on Pd/C nano-composite consisting of Pd octahedron enclosed by (1 1 1) was successfully fabricated by the inkjet printing method, and it demonstrated a high sensitivity of 0.1%, a short response/recover time of 35.5/40.2 s to 4000 ppm H_2 and a great stability (15 cycles) at room temperature. According to the theoretical and experimental results, we propose that the charge transfer from Pd to H resulted from the dissociative adsorption of H_2 on the Pd surfaces, the formation of PdH_x and the interaction between Pd nanoparticles and carbon black lead to the rapid resistance change and make Pd(1 1 1) a superior surface for H_2 sensing. As a fundamental study, this finding achieves deep understanding on the structure-performance correlation of Pd surface structure for H_2 sensing, and it provides a new approach to rationally develop high-performance H_2 sensors.

CRediT authorship contribution statement

Yang Gao: Conceptualization, Methodology, Writing – original draft. **Qiao Lu:** Investigation, Data curation, Writing – original draft. **Peijian Yan:** Resources. **Pengfei Tian:** Methodology, Writing – review & editing, Supervision. **Minghui Zhu:** Resources. **Biao Xiao:** Resources. **Fuzhen Xuan:** Supervision, Project administration, Funding acquisition.

Declaration of Competing Interest

The authors declare that they have no known competing financial interests or personal relationships that could have appeared to influence the work reported in this paper.

References

[1] I. Staffell, D. Scamman, A. Velazquez Abad, P. Balcombe, P.E. Dodds, P. Ekins, N. Shah, K.R. Ward, The role of hydrogen and fuel cells in the global energy system, Energy Environ. Sci. 12 (2019) 463–491.

[2] H. Gu, Z. Wang, Y. Hu, Hydrogen gas sensors based on semiconductor oxide nanostructures, Sensors (Basel) 12 (2012) 5517–5550.

[3] T. Hübert, L. Boon-Brett, G. Black, U. Banach, Hydrogen sensors – A review, Sens. Actuators B: Chem. 157 (2011) 329–352.

[4] S. Öztürk, N. Kılınç, Pd thin films on flexible substrate for hydrogen sensor, J. Alloy. Compd. 674 (2016) 179–184.

[5] J.-H. Kim, A. Mirzaei, H. Woo Kim, P. Wu, S.S. Kim, Design of supersensitive and selective ZnO-nanofiber-based sensors for H_2 gas sensing by electron-beam irradiation, Sens. Actuators B: Chem. 293 (2019) 210–223.

[6] J. Sinay, T. Brestovič, J. Marković, J. Glatz, M. Gorzás, M. Vargová, Analysis of the risks of hydrogen leakage from hydrogen-powered cars and their possible impact on automotive market share increase, Applied Sciences 10 (2020) 4292.

[7] Y. Tamura, M. Takeuchi, K. Sato, Effectiveness of a blower in reducing the hazard of hydrogen leaking from a hydrogen-fueled vehicle, Int. J. Hydrogen Energy 39 (2014) 20339–20349.

[8] J.-H. Yoon, B.-J. Kim, J.-S. Kim, Design and fabrication of micro hydrogen gas sensors using palladium thin film, Mater. Chem. Phys. 133 (2012) 987–991.

[9] C. Wadell, F.A. Nugroho, E. Lidstrom, B. Iandolo, J.B. Wagner, C. Langhammer, Hysteresis-free nanoplasmonic Pd-Au alloy hydrogen sensors, Nano Lett. 15 (2015) 3563–3570.

[10] L. Xie, Z. Li, L. Sun, B. Dong, Q. Fatima, Z. Wang, Z. Yao, A.A. Haidry, Sol-gel synthesis of TiO_2 with p-type response to hydrogen gas at elevated temperature, Front. Mater. 6 (2019) 96.

[11] A. Gupta, S. Gangopadhyay, K. Gangopadhyay, S. Bhattacharya, Palladium-functionalized nanostructured platforms for enhanced hydrogen sensing, Nanomater. Nanotechnol. 6 (2016) 40.

[12] J.-H. Kim, A. Mirzaei, H. Woo Kim, S.S. Kim, Combination of Pd loading and electron beam irradiation for superior hydrogen sensing of electrospun ZnO nanofibers, Sens. Actuators, B 284 (2019) 628–637.

[13] C. wang, A. Mandelis, J.A. Garcia, Pd/PVDF thin film hydrogen sensor system based on photopyroelectric, Sens. Actuators B: Chem. 20 (1999) 228–237.

[14] G. Behzadi Pour, L., Fekri Aval, Monitoring of hydrogen concentration using capacitive nanosensor in a 1% H_2–N_2 mixture, Micro & Nano Lett. 13 (2018) 149–153.

[15] Y.S.H. Najjar, Hydrogen leakage sensing and control (review), Biomed. J. Sci. & Tech. Res. 21 (2019) 16228–16240.

[16] Y. Im, C. Lee, R. Vasquez, M. Bangar, N. Myung, E. Menke, R. Penner, M. Yun, Investigation of a single Pd nanowire for use as a hydrogen sensor, Small 2 (3) (2006) 356–358.

[17] K.J. Jeon, J.M. Lee, E. Lee, W. Lee, Individual Pd nanowire hydrogen sensors fabricated by electron-beam lithography, Nanotechnology 20 (13) (2009) 135502.

[18] A. Boudiba, C. Zhang, P. Umek, C. Bittencourt, R. Snyders, M.-G. Olivier, M. Debliquy, Sensitive and rapid hydrogen sensors based on Pd–WO_3 thick films with different morphologies, Int. J. Hydrogen Energy 38 (5) (2013) 2565–2577.

[19] J.-H. Kim, A. Mirzaei, H.W. Kim, S.S. Kim, Pd functionalization on ZnO nanowires for enhanced sensitivity and selectivity to hydrogen gas, Sens. Actuators B: Chem. 297 (2019) 126693.

[20] Y. Sun, H.H. Wang, High-performance, flexible hydrogen sensors that use carbon nanotubes decorated with palladium nanoparticles, Adv. Mater. 19 (19) (2007) 2818–2823.

[21] H. Hashtroudi, R. Kumar, R. Savu, S. Moshkalev, G.o. Kawamura, A. Matsuda, M. Shafiei, Hydrogen gas sensing properties of microwave-assisted 2D Hybrid Pd/rGO: effect of temperature, humidity and UV illumination, Int. J. Hydrogen Energy 46 (10) (2021) 7653–7665.

[22] J. Panchompoo, L. Aldous, C. Downing, A. Crossley, R.G. Compton, Facile Synthesis of Pd Nanoparticle Modified Carbon Black for Electroanalysis: application to the Detection of Hydrazine, Electroanalysis 23 (7) (2011) 1568–1578.

[23] B. Sharma, J.-S. Kim, Pd/Ag alloy as an application for hydrogen sensing, Int. J. Hydrogen Energy 42 (40) (2017) 25446–25452.

[24] I. Darmadi, F.A.A. Nugroho, S. Kadkhodazadeh, J.B. Wagner, C. Langhammer, Rationally designed PdAuCu ternary alloy nanoparticles for intrinsically deactivation-resistant ultrafast plasmonic hydrogen sensing, ACS Sens. 4 (5) (2019) 1424–1432.

[25] W.-T. Koo, H.-J. Cho, D.-H. Kim, Y.H. Kim, H. Shin, R.M. Penner, I.-D. Kim, Chemiresistive hydrogen sensors: fundamentals, recent advances, and challenges, ACS Nano 14 (11) (2020) 14284–14322.

[26] I. Darmadi, F.A.A. Nugroho, C. Langhammer, High-performance nanostructured palladium-based hydrogen sensors-current limitations and strategies for their mitigation, ACS Sens. 5 (11) (2020) 3306–3327.

[27] H. Cui, P. Jia, X. Peng, Adsorption of SO_2 and NO_2 molecule on intrinsic and Pd-doped $HfSe_2$ monolayer: a first-principles study, Appl. Surf. Sci. 513 (2020) 145863.

[28] H. Cui, X. Zhang, G. Zhang, J.u. Tang, Pd-doped MoS_2 monolayer: a promising candidate for DGA in transformer oil based on DFT method, Appl. Surf. Sci. 470 (2019) 1035–1042.

[29] L. Wang, W. Li, Y. Cai, P. Pan, J. Li, G. Bai, J. Xu, Characterization of Pt- or Pd-doped graphene based on density functional theory for H_2 gas sensor, Mater. Res. Express 6 (9) (2019) 095603.

[30] J. Cheng, D. Hu, A. Yao, Y. Gao, H. Asadi, A computational study on the Pd-decorated ZnO nanocluster for H_2 gas sensing: A comparison with experimental results, Physica E 124 (2020) 114237, https://doi.org/10.1016/j.physe.2020.114237.

[31] T. Kiefer, F. Favier, O. Vazquez-Mena, G. Villanueva, J. Brugger, A single nanotrench in a palladium microwire for hydrogen detection, Nanotechnology 19 (12) (2008) 125502.

[32] L. Du, L. Zheng, H. Wei, S. Zheng, Z. Zhu, J. Chen, D. Yang, Palladium/bismuth nanowires with rough surface for stable hydrogen sensing at low temperatures, ACS Appl. Nano Mater. 2 (3) (2019) 1178–1184.

[33] J. Lee, W. Shim, J.-S. Noh, W. Lee, Design rules for nanogap-based hydrogen sensors, ChemPhysChem 13 (6) (2012) 1395–1403.

[34] Q. Fu, Y. Luo, Active sites of Pd-doped flat and stepped Cu(111) surfaces for H_2 dissociation in heterogeneous catalytic hydrogenation, ACS Catal. 3 (6) (2013) 1245–1252.

[35] H. Abir, M. Sheintuch, Modeling H_2 transport through a Pd or Pd/Ag membrane, and its inhibition by co-adsorbates, from first principles, J. Membr. Sci. 466 (2014) 58–69.

[36] S. Cao, H. Li, Y. Li, B. Zhu, J. Yu, Dependence of exposed facet of Pd on photocatalytic H_2-production activity, ACS Sustain. Chem. Eng. 6 (5) (2018) 6478–6487.

[37] H.J. Monkhorst, J.D. Pack, Special points for Brillouin-zone integrations, Phys. Rev. B 13 (12) (1976) 5188–5192.

[38] W. Tang, E. Sanville, G. Henkelman, A grid-based Bader analysis algorithm without lattice bias, J. Phys. Condens. Matter 21 (8) (2009) 084204.

[39] H. Zhang, T. Watanabe, M. Okumura, M. Haruta, N. Toshima, Catalytically highly active top gold atom on palladium nanocluster, Nat. Mater. 11 (1) (2012) 49–52.

[40] H. Yu, W. Tang, K. Li, H. Yin, S. Zhao, S. Zhou, Design of Cu-based intermetallic nanocrystals for enhancing hydrogenation selectivity, Chem. Eng. Sci. 196 (2019) 402–413.

[41] P. Li, Q. Hong, T. Wu, H. Cui, SOF_2 sensing by Rh-doped PtS_2 monolayer for early diagnosis of partial discharge in the SF_6 insulation device, Mol. Phys. 119 (11) (2021) e1919774.

[42] D. Zhang, Y.e. Sun, C. Jiang, Y. Zhang, Room temperature hydrogen gas sensor based on palladium decorated tin oxide/molybdenum disulfide ternary hybrid via hydrothermal route, Sens. Actuators B: Chem. 242 (2017) 15–24.

[43] J. Xia, Y. Fu, G. He, X. Sun, X. Wang, Core-shell-like Ni-Pd nanoparticles supported on carbon black as a magnetically separable catalyst for green Suzuki-Miyaura coupling reactions, Appl. Catal. B 200 (2017) 39–46.

[44] H. Qian, H. Huang, X. Wang, Design and synthesis of palladium/graphitic carbon nitride/carbon black hybrids as high-performance catalysts for formic acid and methanol electrooxidation, J. Power Sources 275 (2015) 734–741.

[45] J. Wang, S.-Q. Wang, Surface energy and work function of fcc and bcc crystals: density functional study, Surf. Sci. 630 (2014) 216–224.

[46] S. Halas, T. Durakiewicz, Is work function a surface or a bulk property? Vacuum 85 (2010) 486–488.

[47] Z. Zhu, C. Liu, F. Jiang, J. Liu, X. Ma, P. Liu, J. Xu, L. Wang, R. Huang, Flexible and lightweight $Ti_3C_2T_x$ MXene@Pd colloidal nanoclusters paper film as novel H_2 sensor, J Hazard Mater 399 (2020) 123054.

[48] V. Singh, S. Dhall, A. Kaushal, B.R. Mehta, Room temperature response and enhanced hydrogen sensing in size selected Pd-C core-shell nanoparticles: role of carbon shell and Pd-C interface, Int. J. Hydrogen Energy 43 (2) (2018) 1025–1033.

[49] R. Kumar, S. Malik, B.R. Mehta, Interface induced hydrogen sensing in Pd nanoparticle/graphene composite layers, Sens. Actuators, B 209 (2015) 919–926.

[50] J.M. Jeon, T.L. Kim, Y.S. Shim, Y.R. Choi, S. Choi, S. Lee, K.C. Kwon, S.H. Hong, Y.W. Kim, S.Y. Kim, M. Kim, H.W. Jang, Microscopic evidence for strong interaction between Pd and graphene oxide that results in metal-decoration-induced reduction of graphene oxide, Adv. Mater. 29 (2017) 1605929.

[51] Y.M. Wong, W.P. Kang, J.L. Davidson, A. Wisitsora-at, K.L. Soh, A novel microelectronic gas sensor utilizing carbon nanotubes for hydrogen gas detection, Sens. Actuators B: Chem. 93 (2003) 327–332.